

The Study of Dust Formation of Six Tidal Disruption Events

XIAN-MAO CAO (曹先茂),¹ SHAN-QIN WANG (王善钦),¹ WEN-PEI GAN (甘文沛),^{1,2} AND JING-YAO LI (李京谣)¹

¹*Guangxi Key Laboratory for Relativistic Astrophysics, School of Physical Science and Technology, Guangxi University, Nanning 530004, China*

²*Nanjing Institute of Astronomical Optics & Technology, Nanjing 210042, China*

ABSTRACT

This paper investigates eleven (UV-)optical-infrared (IR) spectral energy distributions (SEDs) of six tidal disruption events (TDEs), which are ASASSN-14li, ASASSN-15lh, ASASSN-18ul, ASASSN-18zj, PS18kh, and ZTF18acaqdaa. We find that all the SEDs show evident IR excesses. We invoke the blackbody plus dust emission model to fit the SEDs, and find that the model can account for the SEDs. The derived masses of the dust surrounding ASASSN-14li, ASASSN-15lh, ASASSN-18ul, ASASSN-18zj, PS18kh, and ZTF18acaqdaa are respectively $\sim 0.7 - 1.0 (1.5 - 2.2) \times 10^{-4} M_{\odot}$, $\sim 0.6 - 3.1 (1.4 - 6.3) \times 10^{-2} M_{\odot}$, $\sim 1.0 (2.8) \times 10^{-4} M_{\odot}$, $\sim 0.1 - 1.6 (0.3 - 3.3) \times 10^{-3} M_{\odot}$, $\sim 1.0 (2.0) \times 10^{-3} M_{\odot}$, and $\sim 1.1 (2.9) \times 10^{-3} M_{\odot}$, if the dust is graphite (silicate). The temperature of the graphite (silicate) dust of the six TDEs are respectively $\sim 1140 - 1430 (1210 - 1520)$ K, $\sim 1030 - 1380 (1100 - 1460)$ K, $\sim 1530 (1540)$ K, $\sim 960 - 1380 (1020 - 1420)$ K, $\sim 900 (950)$ K, and $\sim 1600 (1610)$ K. By comparing the derived temperatures to the vaporization temperature of graphite (~ 1900 K) and silicate ($\sim 1100 - 1500$ K), we suggest that the IR excesses of PS18kh can be explained by both the graphite and silicate dust, the rest five TDEs favor the graphite dust while the silicate dust model cannot be excluded. Moreover, we demonstrate the lower limits of the radii of the dust shells surrounding the six TDEs are significantly larger than those of the radii of the photospheres at the first epochs of SEDs, indicating that the dust might exist before the the TDEs occurred.

Keywords: circumstellar matter – dust – Tidal Disruption Events: general – Tidal Disruption Events: individual (ASASSN-14li, ASASSN-15lh, ASASSN-18ul, ASASSN-18zj, PS18kh, ZTF18acaqdaa)

1. INTRODUCTION

Supermassive black holes in the centers of galaxies can disrupt stars, and produce the tidal disruption events (TDEs, Hills 1975; Rees 1988; van Velzen et al. 2016; Gezari 2021), which emit luminous multi-band radiation (Frederick et al. 2019). Generally, the X-ray and optical light curves of TDEs follow a power-law function ($F_{\nu} \propto t^{-5/3}$) which reflects the evolution of the accretion rate. The spectral energy distributions (SEDs) of most TDEs can be well described by the blackbody function, while the SEDs of some TDEs cannot be fitted by the blackbody function and show evident infrared (IR) excesses relative to the blackbody SEDs (e.g., Dou et al. 2016; Jiang et al. 2016; Dou et al. 2017; Jiang et al. 2017, 2019).

It is widely believed that the IR excesses of SEDs of TDEs, SNe, as well as other optical transients can be explained by the dust emission. In this scenario, the UV and optical emission from the photospheres of the transients heat the dust surrounding them, and the heated dust emit flux peaked at IR bands and produce IR excesses. The flux from the photospheres and the dust shells yield SEDs with IR excesses relative the blackbody SEDs. Studying the IR excesses of the SEDs of TDEs would help to infer the masses, temperature, chemical composition, and locations of the dust grains.

Based on the observations of W_1 ($3.4 \mu\text{m}$) and W_2 ($4.6 \mu\text{m}$) of *Wide-field Infrared Survey Explorer (WISE)* and the optical data obtained by optical telescopes, Jiang et al. (2016) construct 3 optical-IR SEDs of ASASSN-14li, and use

double-blackbody model to derive temperatures of the dust at different epochs by fitting the SEDs. The derived value dust temperature at MJD ≈ 57019 is 2091 ± 172 K. [Jiang et al. \(2017\)](#) use double-blackbody model and blackbody plus dust model to fit the optical-IR SED of PS16dtm at MJD $\approx 57,755$, finding that the dust temperature is 1180 K (for the former model) or 700 K (for the later model).

[Jiang et al. \(2021\)](#) collect a sample of TDEs observed by *WISE* at the filters of W_1 and W_2 . To subtract the flux from the photospheres of the TDEs, they adopt the evolution pattern of the photosphere bolometric luminosity obtained by [van Velzen et al. \(2020\)](#), and assume that the temperature of the TDEs keep constant to be the averaged values of the first 100 days. After subtracting the flux from the photospheres in W_1 - and W_2 - bands, [Jiang et al. \(2021\)](#) get the IR excesses at all epochs for all *WISE*-selected TDEs. They invoke the dust model to fit the IR excesses of the SEDs of TDEs and derive the physical parameters (temperature, luminosity, radii of the dust shell, covering factor, etc.) of the dust.

In this paper, we combine the IR (W_1 , W_2) photometry of six TDEs provided by [Jiang et al. \(2021\)](#) with the (UV-)optical photometry of the same TDEs at the same epochs, constructing the (UV-)optical-IR SEDs and fit the SEDs by using the blackbody model to test if the SEDs of the six TDEs show IR excesses. For the SEDs showing IR excesses, we use blackbody plus dust emission model to fit them, and constrain the physical properties of the dust. This method does not depend on any assumptions about the bolometric luminosity and the temperature evolution.

The paper is organized as follow. In section 2, we use the single-component model and double-component model to fit the SEDs of the six TDEs. We discuss our results and draw some conclusions in Sections 3 and 4, respectively.

2. THE OPTICAL AND IR SEDS AND THE SED FITTING

In this section, we study the SEDs of the six TDEs (ASASSN-14li, ASASSN-15lh, ASASSN-18ul, ASASSN-18zj, PS18kh, and ZTF18acaqdaa) having optical-IR SEDs. The information of the six TDEs is listed in Table 1. The IR photometry of all the six TDEs are from Table 2 of [Jiang et al. \(2021\)](#). The sources of the (UV-)optical photometry of the TDEs are also listed in Table 1.

Combining the IR (W_1 , W_2) photometry of [Jiang et al. \(2021\)](#) with the (UV-)optical photometry, we obtain eleven SEDs of ASASSN-14li (3 SEDs), ASASSN-15lh (3 SEDs)¹, ASASSN-18ul (1 SED), ASASSN-18zj (2 SEDs), PS18kh (1 SED), and ZTF18acaqdaa (1 SED).

First, we fit the SEDs of the TDEs using the blackbody model, in which the flux from the photosphere ($F_{\nu, \text{ph}}$) is $\pi B_{\nu}(T_{\text{ph}})R_{\text{ph}}^2/D_L^2$, where $B_{\nu}(T_{\text{ph}}) = (2h\nu^3/c^2)(e^{\frac{h\nu}{k_b T_{\text{ph}}}} - 1)^{-1}$ is the intensity of the blackbody radiation of the photosphere, R_{ph} , T_{ph} , and D_L are the radius, temperature of the photosphere, and the luminosity distance of a TDE, respectively. The free parameters of the model are the radius (R_{ph}) and the temperature (T_{ph}) of the TDE photosphere. The Markov Chain Monte Carlo (MCMC) method using the *emcee* Python package ([Foreman-Mackey et al. 2013](#)) was adopted to get best-fitting parameters and the $1-\sigma$ range of the parameters.

The blackbody fits for the SEDs of the six TDEs and the corresponding best-fitting parameters of the model are shown in Figure 1 and Table 2, respectively. Figure 1 indicates that all the SEDs of the six TDEs show evident IR excesses relative to the blackbody SEDs.

To fit the SEDs, we assume that the IR excesses are due to the emission from the dust heated by the UV and optical emission of the TDE photospheres, and invoke the blackbody plus dust emission model to fit the SEDs. We suppose that the dust can be either graphite or silicate, and adopt a power-law grain size distribution function $f(a) \propto a^{-\alpha}$ ($\int_{a_{\text{min}}}^{a_{\text{max}}} f(a) da = 1$) [Gall et al. 2014](#)). To compare the results with those of [Jiang et al. \(2021\)](#), the values of α , a_{min} , and a_{max} in this paper are set to be 3.5, $0.01 \mu\text{m}$, and $10 \mu\text{m}$, respectively.

Assuming that the number of the dust grains having a radius of a is $N_d(a)$, the total mass of the dust $M_d = \int_{a_{\text{min}}}^{a_{\text{max}}} N_d(a)m_d(a)da = N_d \int_{a_{\text{min}}}^{a_{\text{max}}} f(a)m_d(a)da$ (m_d is the the mass of a dust grain with a radius of a), the flux from the dust is $\int_{a_{\text{min}}}^{a_{\text{max}}} [\pi B_{\nu}(T_d)Q_{\nu}(a)]4\pi a^2 N(a)da/4\pi D_L^2 = N_d/D_L^2 \int_{a_{\text{min}}}^{a_{\text{max}}} f(a)m(a)\kappa_{\nu}(a)B_{\nu}(T_d)da$ (since $\kappa_{\nu}(a) = \frac{3Q_{\nu}(a)}{4\rho a}$, $m(a) = 4/3\pi\rho a^3$). Here, T_d is the temperature of the dust; $\kappa_{\nu}(a)$ is the mass absorption coefficient of the dust grains (see [Gan et al. 2021](#) and the references therein for more details). The free parameters of the blackbody plus dust emission model are R_{ph} , T_{ph} , T_d , and M_d .

The best-fitting blackbody plus graphite (or silicate) dust model for the SEDs and the corresponding best-fitting parameters (masses and temperature) of the model are shown in Figure 2 and Table 3, respectively. We find that

¹ It should be noted that the nature of ASASSN-15lh is still in debate. [Dong \(2016\)](#) suggest that it is a superluminous SN, while [Leloudas \(2016\)](#) argue that it is a TDE.

the model can explain the SEDs of the six TDEs. The derived masses of the graphite (silicate) dust of ASASSN-14li, ASASSN-15lh, ASASSN-18ul, ASASSN-18zj, PS18kh, and ZTF18acaqdaa are $\sim 0.7 - 1.0 (1.5 - 2.2) \times 10^{-4} M_{\odot}$, $\sim 0.6 - 3.1 (1.4 - 6.3) \times 10^{-2} M_{\odot}$, $\sim 1.0 (2.8) \times 10^{-4} M_{\odot}$, $\sim 0.1 - 1.6 (0.3 - 3.3) \times 10^{-3} M_{\odot}$, $\sim 1.0 (2.0) \times 10^{-3} M_{\odot}$, and $\sim 1.1 (2.9) \times 10^{-3} M_{\odot}$, respectively. The derived temperatures of the graphite (silicate) dust of the six TDEs are $\sim 1140 - 1430 (1210 - 1520)$ K, $\sim 1030 - 1380 (1100 - 1460)$ K, $\sim 1530 (1540)$ K, $\sim 960 - 1380 (1020 - 1420)$ K, $\sim 900 (950)$ K, and $\sim 1600 (1610)$ K, respectively. The derived dust masses of the silicate are about two to three times those of the graphite dust. Moreover, the derived mass of the dust of ASASSN-15lh is $(0.6 - 3.1) (1.4 - 6.3) \times 10^{-2} M_{\odot}$, which is one or two magnitudes larger than those of other five TDEs.

We plot the evolution of the masses and the temperatures of the dust in Figure 3. For comparison, the temperatures of the dust of four TDEs (ASASSN-14li, ASASSN-15lh, PS18kh, ASASSN-18zj) derived by Jiang et al. (2021) are also presented in the same Figure 3.

We find that the derived temperatures of graphite dust of the six TDEs are reasonable, since they are lower than the vaporization temperature of graphite $T_{\text{vap,g}}$ (~ 1900 K, e.g., Stritzinger et al. 2012). The silicate dust cannot explain the IR excesses of ASASSN-18ul and ZTF18acaqdaa since the derived temperatures are higher than the vaporization temperature of silicate $T_{\text{vap,s}}$ ($\sim 1100 - 1300$ K, Mattila et al. 2008; or ~ 1500 K, Gall et al. 2014); the IR excesses of ASASSN-14li, ASASSN-15lh and ASASSN-18zj can be narrowly explained by the silicate dust since the derived temperatures are around the upper limit of $T_{\text{vap,s}}$. IR excess of PS18kh can be due to the silicate dust emission. Due to the uncertainty of the lower limit of $T_{\text{vap,s}}$, we favor the graphite model, though the silicate model cannot be excluded for some events.

3. DISCUSSION

3.1. The luminosity and the lower limit of the radii of the dust shells

Using the equations in Fox et al. (2011), we calculate the luminosity and the blackbody radii ($R_{\text{bb,d}}$) of the dust shells which are the lower limits of the dust shell radii, see Table 4 and Figure 4.

By comparing R_{ph} and $R_{\text{bb,d}}$ of the TDEs at the first epochs when the optical-IR SEDs are available, we can infer the origin of the dust. Combining Tables 2 and 4, we find that R_{ph} ($R_{\text{bb,d}}$) of ASASSN-14li at day 29, ASASSN-15lh at day 112, ASASSN-18ul at day 95, ASASSN-18zj at day 21, PS18kh at day 17, ZTF18acaqdaa at day 91 are $\sim 1.9 \times 10^{14}$ cm ($\sim 1.1 \times 10^{16}$ cm), $\sim 2.2 \times 10^{15}$ cm ($\sim 8.4 \times 10^{16}$ cm), $\sim 3.7 \times 10^{14}$ cm ($\sim 1.2 \times 10^{16}$ cm), $\sim 1.4 \times 10^{15}$ cm ($\sim 3.8 \times 10^{16}$ cm), $\sim 1.6 \times 10^{15}$ cm ($\sim 2.8 \times 10^{16}$ cm), $\sim 4.8 \times 10^{15}$ cm ($\sim 3.8 \times 10^{16}$ cm), respectively. The $R_{\text{bb,d}}$ values are respectively 58, 38, 32, 27, 18, and 8 times the R_{ph} values for ASASSN-14li, ASASSN-15lh, ASASSN-18ul, ASASSN-18zj, PS18kh, and ZTF18acaqdaa, indicating that the dust shells are formed prior the TDE occurred.

3.2. Comparison to the results in the literature

Jiang et al. (2021) assume that the dust is silicate and find that the temperature of ASASSN-14li and ASASSN-15lh is ~ 1400 K, the temperature of PS18kh and ASASSN-18zj is ~ 1000 K. Our derived temperatures of the dust of the four TDEs are consistent with those of Jiang et al. (2021), see the right panel of Figure 3. This supports the conclusion that the four TDEs show evident IR excesses. Our derived luminosities of the dust of the four TDEs are also consistent with those of Jiang et al. (2021), see the left panel of Figure 4. Additionally, we obtain the temperatures and luminosities of the dust of ASASSN-18ul and ZTF18acaqdaa, while they are absent in the literature.

The consistency between our results and Jiang et al. (2021)'s results might be due to the fact that the two assumptions adopted by Jiang et al. (2021) are valid, or the fact that the IR flux from the hot photospheres of the TDEs are (significantly) lower than that from the cool dust and the results are insensitive to the bolometric light-curve and temperature evolution patterns assumed.

4. CONCLUSIONS

In this paper, we collect the (UV-)optical and IR data of six TDEs (ASASSN-14li, ASASSN-15lh, ASASSN-18ul, ASASSN-18zj, PS18kh, and ZTF18acaqdaa) from the literature, constructing and fitting their optical-IR SEDs at different epochs. The blackbody model fits show that the SEDs of the all six TDEs show IR excesses, while the blackbody plus dust emission model can account for the SEDs showing IR excesses.

The fits using the blackbody plus dust emission model show that the IR excesses of ASASSN-14li, ASASSN-15lh, ASASSN-18ul, ASASSN-18zj, PS18kh, and ZTF18acaqdaa are produced by the graphite (silicate) dust of the masses of $\sim 0.7 - 1.0 (1.5 - 2.2) \times 10^{-4} M_{\odot}$, $\sim 0.6 - 3.1 (1.4 - 6.3) \times 10^{-2} M_{\odot}$, $\sim 1.0 (2.8) \times 10^{-4} M_{\odot}$, $\sim 0.1 - 1.6 (0.3 - 3.3) \times 10^{-3} M_{\odot}$,

$\sim 1.0 (2.0) \times 10^{-3} M_{\odot}$, and $\sim 1.1 (2.9) \times 10^{-3} M_{\odot}$, respectively. The derived temperatures of the graphite (silicate) dust of them are $\sim 1140-1430 (1210-1520)$ K, $\sim 1030-1380 (1100-1460)$ K, $\sim 1530 (1540)$ K, $\sim 960-1380 (1020-1420)$ K, $\sim 900 (950)$ K, and $\sim 1600 (1610)$ K, respectively.

By comparing the derived temperatures to the vaporization temperature of graphite (~ 1900 K) and silicate ($\sim 1100 - 1500$ K), we suggest that the IR excesses of PS18kh can be explained by both the graphite and silicate dust, the rest five TDEs favor the graphite dust while the silicate dust model cannot be excluded.

Moreover, we calculate the dust luminosities (L_{ph}) and the blackbody radii ($R_{\text{bb,d}}$) which are the lower limits of the dust shells, finding that $R_{\text{bb,d}}$ of the six TDEs are tens or hundreds of times R_{ph} at the epochs when their first SEDs are available. This indicates that the IR excesses of the TDEs are produced by the pre-existing dust.

The advantage of our method is that it does not depend on any assumptions of evolution patterns of bolometric luminosities and temperatures. On the other hand, however, its disadvantage is that they are fewer epochs when (UV-)optical and IR photometry are available. We expected that (UV-)optical and IR observations for TDEs in the future can provide more (UV-)optical-IR SEDs for individual events that can be used to constrain the properties of the dust.

ACKNOWLEDGMENTS

This work is supported by National Natural Science Foundation of China (grant 11963001).

Table 1. The information of the six TDEs in the sample.

Name	R.A. (J2000)	Decl. (J2000)	Redshift	Discovery date	Obs. Filters	References ^a
ASASSN-14li	12 ^h 48 ^m 15 ^s .23	+17°46′26″.4	0.0206	Nov 22 2014	<i>UVW2, UVM2, UVW1, r, B, V, g, U, i, W1, W2</i>	1, 2
ASASSN-15lh	22 ^h 02 ^m 15 ^s .39	−61°39′34″.6	0.2326	Jun 14 2015	<i>UVW2, UVM2, UVW1, g, i, r, B, V, U, W1, W2</i>	1, 3, 4
ASASSN18ul	22 ^h 50 ^m 16 ^s .064	−44°51′53″.26	0.059	Sep 08 2018	<i>UVW2, UVM2, UVW1, U, B, V, W1, W2</i>	1, 5
ASASSN18zj	10 ^h 06 ^m 50 ^s .871	+01°41′34″.08	0.04573	Dec 14 2018	<i>UVW2, UVM2, UVW1, U, B, g, r, i, W1, W2</i>	1, 6
PS18kh	07 ^h 56 ^m 54 ^s .54	+34°15′43″.6	0.0710	Feb 07 2018	<i>g, r, o, B, V, W1, W2</i>	1, 7
ZTF18acaqdaa	17 ^h 28 ^m 03 ^s .93	+30°41′31″.4	0.2120	Nov 11 2018	<i>g, r, W1, W2</i>	1, 8

^a References. (1) Jiang et al. (2021); (2) Holoien et al. (2016); (3) Godoy-Rivera et al. (2017); (4) Leloudas (2016); (5) Wevers, T. (2019); (6) Gomez et al. (2020); (7) Holoien (2019); (8) *MARS* (<https://mars.lco.global>).

Table 2. The best-fitting parameters of the blackbody model for the SEDs of the six TDEs, including the temperature of the photosphere T_{ph} , the radius of the photosphere R_{ph}

Phase ^a	T_{ph}	R_{ph}	χ^2/dof
(days)	(10^3 K)	(10^{15} cm)	
ASASSN-14li			
29.0 d	$34.00^{+1.34}_{-1.21}$	$0.19^{+0.01}_{-0.01}$	21.95
199.0 d	$51.22^{+25.09}_{-14.83}$	$0.051^{+0.020}_{-0.014}$	10.84
387.0 d	$33.13^{+22.21}_{-9.40}$	$0.072^{+0.040}_{-0.029}$	26.43
ASASSN-15lh			
112.0 d	$20.06^{+3.15}_{-1.46}$	$2.23^{+0.21}_{-0.31}$	15.88
265.0 d	$27.97^{+23.92}_{-8.70}$	$1.02^{+0.47}_{-0.40}$	25.01
405.0 d	$19.26^{+23.91}_{-4.58}$	$0.96^{+0.41}_{-0.50}$	44.99
ASASSN-18ul			
95.0 d	$39.41^{+5.10}_{-3.87}$	$0.37^{+0.04}_{-0.04}$	6.06
ASASSN-18zj			
21.0 d	$16.20^{+0.19}_{-0.19}$	$1.40^{+0.03}_{-0.03}$	30.97
170.0 d	$21.91^{+1.16}_{-1.08}$	$0.30^{+0.02}_{-0.02}$	4.09
PS18kh			
17.0 d	$14.15^{+1.53}_{-1.25}$	$1.62^{+0.18}_{-0.17}$	3.54
ZTF18acaqdaa			
91.0 d	$8.99^{+6.95}_{-1.93}$	$4.80^{+2.68}_{-2.61}$	7.65

^a All the phases are relative to the peak date which are respectively MJD 56989 (ASASSN-14li), MJD 57247 (ASASSN-15lh), MJD 58317 (ASASSN-18ul), MJD 58180 (PS18kh), MJD 58427 (ASASSN-18zj), and MJD 58442 (ZTF18acaqdaa) (see Jiang et al. 2021). All epochs are transformed to the rest-frame ones.

Table 3. The best-fitting parameters (the temperature of the photosphere T_{ph} , the radius of the photosphere R_{ph} , the temperature of the dust shell T_{d} , and the mass of the dust shell M_{d}) of the blackbody plus graphite (silicate) model for the SEDs of the six TDEs.

Phase (days)	Blackbody plus Graphite					Blackbody plus Silicate				
	T_{ph} (10^3 K)	R_{ph} (10^{15} cm)	T_{d} (10^3 K)	M_{d} ($10^{-3} M_{\odot}$)	χ^2/dof	T_{ph} (10^3 K)	R_{ph} (10^{15} cm)	T_{d} (10^3 K)	M_{d} ($10^{-3} M_{\odot}$)	χ^2/dof
ASASSN-14li										
29.0 d	$34.38^{+1.37}_{-1.26}$	$0.19^{+0.01}_{-0.01}$	$1.43^{+0.39}_{-0.28}$	$0.10^{+0.11}_{-0.05}$	6.29	$34.37^{+1.37}_{-1.23}$	$0.19^{+0.01}_{-0.01}$	$1.52^{+0.34}_{-0.30}$	$0.22^{+0.22}_{-0.09}$	6.26
199.0 d	$54.10^{+24.24}_{-16.10}$	$0.049^{+0.019}_{-0.013}$	$1.14^{+0.44}_{-0.28}$	$0.095^{+0.201}_{-0.062}$	0.40	$53.92^{+25.35}_{-15.92}$	$0.049^{+0.019}_{-0.013}$	$1.21^{+0.44}_{-0.31}$	$0.21^{+0.42}_{-0.13}$	0.38
387.0 d	$39.57^{+26.02}_{-12.03}$	$0.059^{+0.031}_{-0.022}$	$1.38^{+0.37}_{-0.30}$	$0.068^{+0.088}_{-0.033}$	0.85	$39.24^{+25.95}_{-11.89}$	$0.059^{+0.032}_{-0.022}$	$1.45^{+0.34}_{-0.31}$	$0.15^{+0.19}_{-0.07}$	0.77
ASASSN-15lh										
112.0 d	$24.33^{+10.87}_{-4.16}$	$1.83^{+0.38}_{-0.50}$	$1.38^{+0.35}_{-0.27}$	$6.08^{+8.45}_{-3.30}$	1.24	$24.31^{+10.85}_{-4.15}$	$1.83^{+0.38}_{-0.50}$	$1.46^{+0.33}_{-0.28}$	$13.87^{+17.07}_{-6.68}$	1.23
265.0 d	$38.09^{+29.45}_{-13.88}$	$0.78^{+0.38}_{-0.26}$	$1.27^{+0.34}_{-0.22}$	$10.55^{+13.51}_{-6.15}$	0.18	$38.27^{+29.61}_{-13.96}$	$0.78^{+0.38}_{-0.26}$	$1.37^{+0.34}_{-0.25}$	$22.35^{+27.77}_{-11.85}$	0.16
405.0 d	$29.40^{+34.00}_{-12.25}$	$0.62^{+0.47}_{-0.27}$	$1.03^{+0.15}_{-0.11}$	$31.14^{+22.72}_{-14.17}$	0.19	$28.82^{+33.52}_{-11.94}$	$0.64^{+0.48}_{-0.28}$	$1.10^{+0.18}_{-0.13}$	$63.10^{+46.81}_{-29.62}$	0.30
ASASSN-18ul										
95.0 d	$40.28^{+5.55}_{-4.04}$	$0.36^{+0.04}_{-0.04}$	$1.53^{+0.32}_{-0.43}$	$0.10^{+0.19}_{-0.05}$	5.61	$40.21^{+5.44}_{-4.05}$	$0.36^{+0.04}_{-0.04}$	$1.54^{+0.32}_{-0.44}$	$0.28^{+0.47}_{-0.13}$	5.67
ASASSN-18zj										
21.0 d	$16.55^{+0.21}_{-0.20}$	$1.34^{+0.03}_{-0.03}$	$0.96^{+0.17}_{-0.11}$	$1.59^{+1.26}_{-0.78}$	10.59	$16.55^{+0.21}_{-0.20}$	$1.34^{+0.03}_{-0.03}$	$1.02^{+0.20}_{-0.13}$	$3.25^{+2.66}_{-1.63}$	10.59
170.0 d	$22.02^{+1.18}_{-1.08}$	$0.30^{+0.02}_{-0.02}$	$1.38^{+0.40}_{-0.41}$	$0.10^{+0.27}_{-0.05}$	1.04	$22.02^{+1.18}_{-1.10}$	$0.30^{+0.02}_{-0.02}$	$1.42^{+0.38}_{-0.40}$	$0.26^{+0.60}_{-0.14}$	1.04
PS18kh										
17.0 d	$15.31^{+1.85}_{-1.49}$	$1.49^{+0.18}_{-0.16}$	$0.90^{+0.61}_{-0.31}$	$0.92^{+8.33}_{-0.81}$	1.55	$15.38^{+1.86}_{-1.50}$	$1.48^{+0.17}_{-0.16}$	$0.95^{+0.59}_{-0.33}$	$1.96^{+17.13}_{-1.68}$	1.55
ZTF18acaqdaa										
91.0 d	$27.48^{+32.60}_{-12.65}$	$1.29^{+1.08}_{-0.56}$	$1.60^{+0.29}_{-0.40}$	$1.06^{+1.65}_{-0.46}$	–	$26.89^{+32.20}_{-12.39}$	$1.31^{+1.12}_{-0.58}$	$1.61^{+0.28}_{-0.39}$	$2.85^{+4.14}_{-1.24}$	–

Table 4. The derived parameters (the photosphere luminosities (L_{ph}), the dust luminosities (L_{d}), and the blackbody radii of the dust shells ($R_{\text{bb,d}}$) of the TDEs of the blackbody plus graphite (silicate) model.

Phase (days)	L_{ph} (10^{42} erg s $^{-1}$)	L_{d} (10^{42} erg s $^{-1}$)	$R_{\text{bb,d}}$ (10^{15} cm)
ASASSN-14li			
29.0 d	$34.82^{+2.89}_{-2.50}$ (34.83 $^{+2.84}_{-2.47}$)	$0.37^{+0.23}_{-0.11}$ (0.40 $^{+0.16}_{-0.09}$)	$11.09^{+3.53}_{-2.32}$ (10.23 $^{+3.82}_{-2.07}$)
199.0 d	$14.40^{+20.54}_{-7.54}$ (14.33 $^{+21.77}_{-7.48}$)	$0.12^{+0.08}_{-0.03}$ (0.15 $^{+0.06}_{-0.03}$)	$9.84^{+5.73}_{-3.22}$ (9.56 $^{+7.17}_{-3.36}$)
387.0 d	$6.08^{+12.21}_{-2.74}$ (5.99 $^{+12.01}_{-2.67}$)	$0.21^{+0.12}_{-0.06}$ (0.23 $^{+0.09}_{-0.05}$)	$9.01^{+3.38}_{-1.97}$ (8.44 $^{+3.81}_{-1.88}$)
ASASSN-15lh			
112.0 d	$510.19^{+48.09}_{-36.57}$ (509.97 $^{+48.10}_{-36.52}$)	$18.91^{+6.76}_{-3.24}$ (21.71 $^{+4.78}_{-3.00}$)	$84.94^{+35.83}_{-22.15}$ (80.10 $^{+37.08}_{-20.42}$)
265.0 d	$156.06^{+7.52}_{-6.31}$ (156.06 $^{+7.54}_{-6.33}$)	$22.30^{+6.70}_{-3.13}$ (26.63 $^{+4.99}_{-3.29}$)	$108.30^{+43.57}_{-31.56}$ (100.80 $^{+47.93}_{-29.35}$)
405.0 d	$55.70^{+3.54}_{-3.38}$ (55.73 $^{+3.66}_{-3.42}$)	$24.47^{+2.16}_{-1.95}$ (30.87 $^{+3.03}_{-2.65}$)	$171.59^{+44.47}_{-38.00}$ (166.84 $^{+53.58}_{-44.27}$)
ASASSN-18ul			
95.0 d	$239.63^{+71.69}_{-43.75}$ (238.61 $^{+70.66}_{-43.51}$)	$0.53^{+0.34}_{-0.24}$ (0.54 $^{+0.28}_{-0.22}$)	$11.81^{+5.61}_{-2.74}$ (11.47 $^{+6.77}_{-2.87}$)
ASASSN-18zj			
21.0 d	$95.82^{+0.99}_{-0.98}$ (95.84 $^{+0.98}_{-0.98}$)	$0.88^{+0.11}_{-0.08}$ (1.17 $^{+0.12}_{-0.10}$)	$37.69^{+10.31}_{-9.02}$ (37.89 $^{+13.55}_{-10.98}$)
170.0 d	$15.21^{+1.65}_{-1.44}$ (15.21 $^{+1.66}_{-1.44}$)	$0.32^{+0.21}_{-0.11}$ (0.36 $^{+0.15}_{-0.10}$)	$11.13^{+7.40}_{-2.84}$ (11.02 $^{+8.56}_{-3.08}$)
PS18kh			
17.0 d	$86.80^{+21.84}_{-15.13}$ (87.38 $^{+22.21}_{-15.22}$)	$0.54^{+0.29}_{-0.21}$ (0.73 $^{+0.50}_{-0.29}$)	$28.17^{+48.01}_{-16.13}$ (29.49 $^{+68.57}_{-17.73}$)
ZTF18acaqdaa			
91.0 d	$674.21^{+4247.29}_{-482.34}$ (642.27 $^{+4065.02}_{-457.19}$)	$6.61^{+3.21}_{-2.61}$ (6.87 $^{+2.66}_{-2.54}$)	$38.00^{+16.62}_{-8.37}$ (37.17 $^{+18.92}_{-8.77}$)

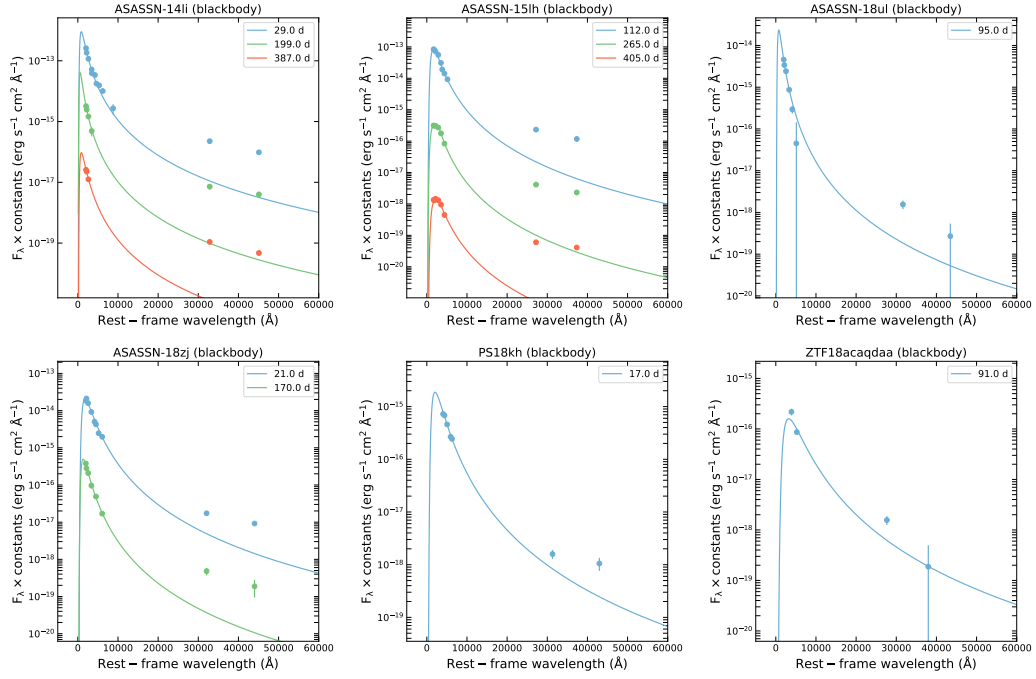


Figure 1. The optical and IR SEDs of ASASSN-14li, ASASSN-15lh, PS18kh, ZTF18acaqdaa, ASASSN-18ul, and ASASSN-18zj and the fits of the blackbody model. For clarity, the flux at all epochs are shifted by multiplying different constants.

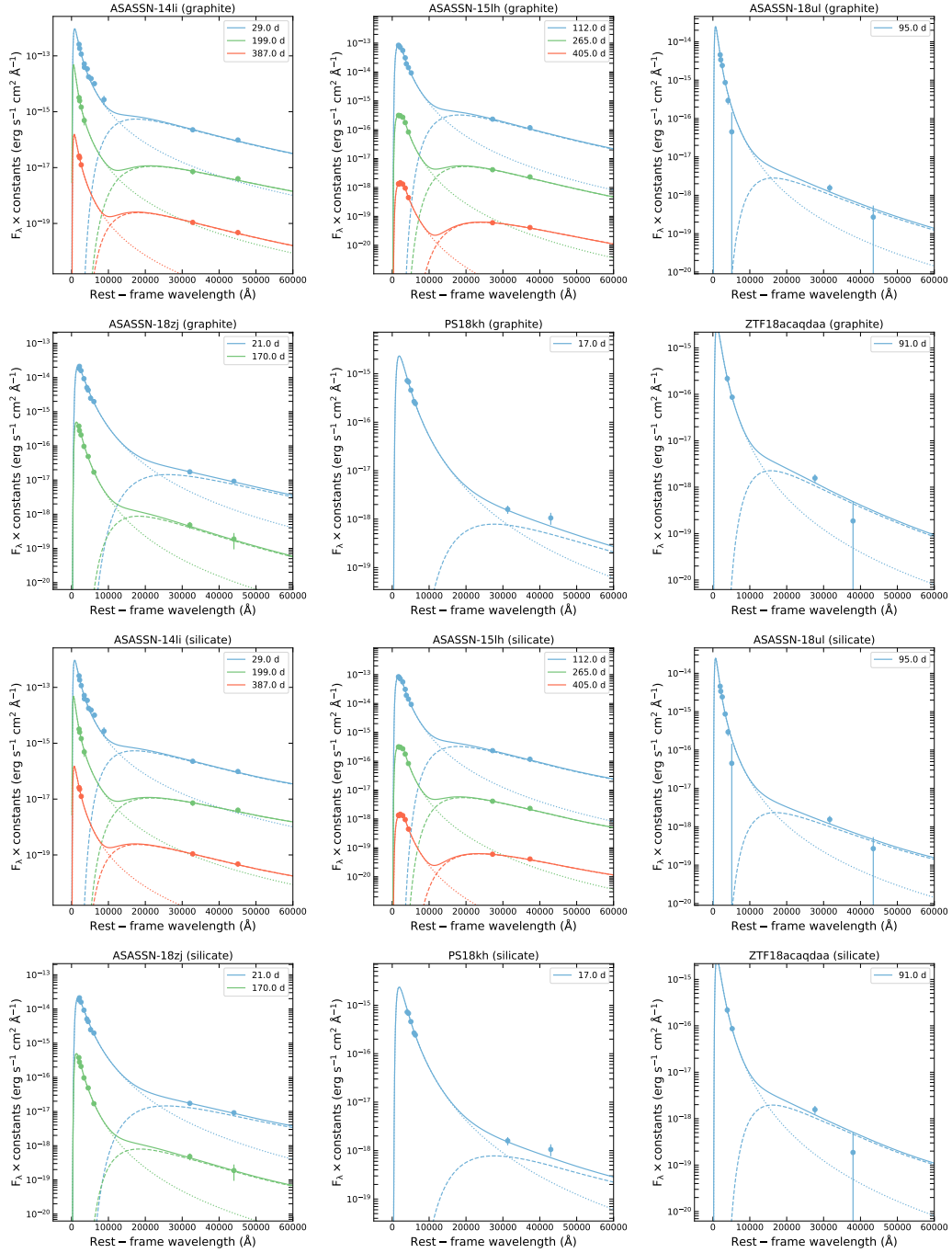


Figure 2. The best-fitting SEDs of ASASSN-14li, ASASSN-15lh, ASASSN-18ul, ASASSN-18zj, PS18kh, and ZTF18acaqdaa obtained by using the blackbody plus graphite (the first two rows) or silicate (the last two rows) model. The dotted, dashed, and solid lines represent the flux of the photospheres, the dust, and the sum of the two components, respectively.

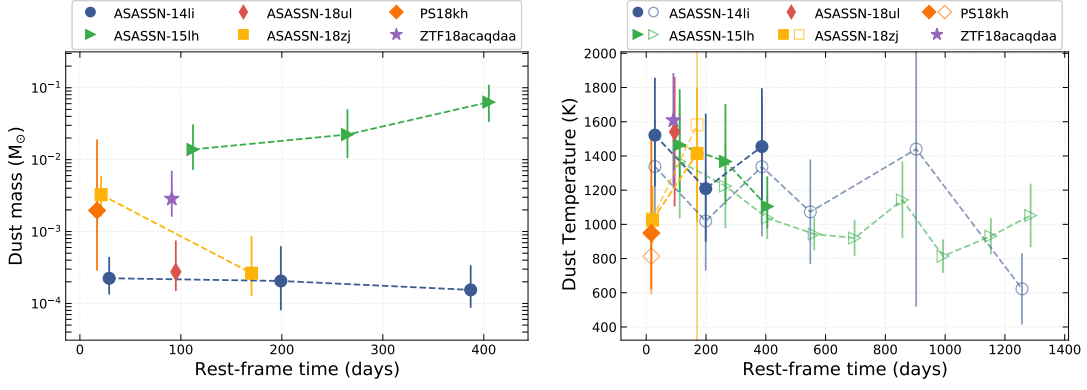


Figure 3. The masses (left panel), the temperatures (right panel) of the dust of the six TDEs. For comparison, the temperatures of the dust derived by Jiang et al. (2021) for four TDEs (ASASSN-14li, ASASSN-15lh, PS18kh, and ASASSN-18zj) are also plotted by the open symbols in the right panel.

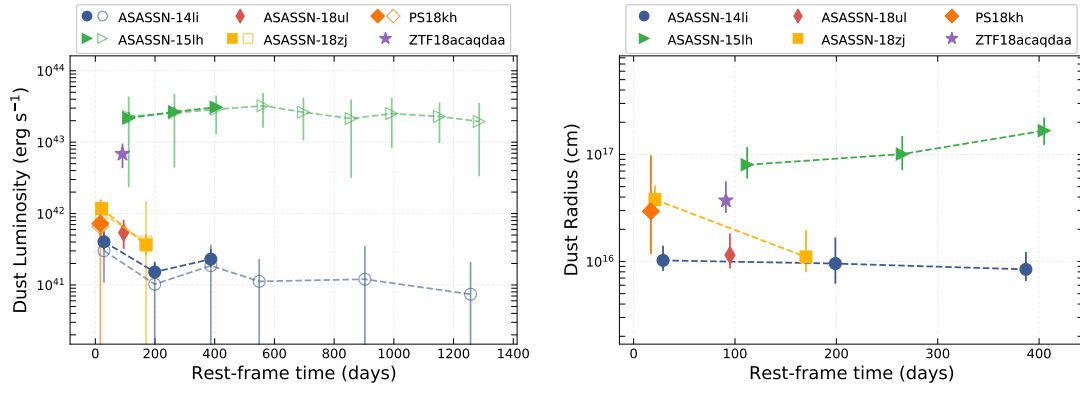


Figure 4. The luminosities (left panel) and the radii (right panel) of the dust shells of the six TDEs. For comparison, the dust luminosities derived by Jiang et al. (2021) for four TDEs (ASASSN-14li, ASASSN-15lh, PS18kh, and ASASSN-18zj) are also plotted by the open symbols in the left panel.

REFERENCES

- Dong, S., Shappee, B. J., Prieto, J. L., et al. 2016, *Science*, 351, 6270
- Dou, L., Wang, T., Jiang, N., et al. 2016, *ApJ*, 832, 188
- Dou, L., Wang, T., Yan, L., et al. 2017, *ApJL*, 841, L8
- Foreman-Mackey, D., Hogg, D. W., Lang, D., et al. 2013, *PASP*, 125, 306
- Fox, O., Chevalier, R., Skrutskie, M., et al. 2011, *ApJ*, 741, 7
- Frederick, S., Gezari, S., Graham, M. J., et al. 2019, *ApJ*, 883, 31
- Gall, C., Hjorth, J., Watson, D., et al. 2014, *Nature*, 511, 326
- Gan, W., Wang, S., & Liang, E. 2021, *ApJ*, 914, 125
- Gezari, S. 2021, 2021, *ARA&A*, 59, 21
- Godoy-Rivera, D., Stanek, K., Kochanek, C., et al. 2017, *MNRAS*, 466, 2
- Gomez, S., Nicholl, M., Philip, S., et al. 2020, *MNRAS*, 497, 1925
- Hills, J. 1975, *Nature*, 254, 5498, 295
- Holoien, T., Kochanek, C., Prieto, J., et al. 2016, *MNRAS*, 455, 2918
- Holoien, T., Huber, M., et al. 2019, *ApJ*, 880, 120
- Jiang, N., Dou, L., Wang, T., et al. 2016, *ApJL*, 828, L14
- Jiang, N., Wang, T., Hu, X., Sun, L., Dou, L., & Xiao, L. 2021, *ApJ*, 911, 31
- Jiang, N., Wang, T., Mou, G., et al. 2019, *ApJ*, 871, 15
- Jiang, N., Wang, T., Yan, L., et al. 2017, *ApJ*, 850, 63
- Leloudas, G., Fraser, M., Stone, N. C., et al. 2016, *NatAs*, 1, 0002
- Mattila, S., Meikle, W., Lundqvist, P., et al. 2008, *MNRAS*, 389, 141
- Rees, M. J. 1988, *Nature*, 333, 6173, 523
- Stritzinger, M., Taddia, F., Fransson, C., et al. 2012, *ApJ*, 756, 173
- van Velzen, S., Mendez, A., Krolik, J., & Gorjian, V. 2016, *ApJ*, 829, 19
- van Velzen, S., Holoien, T., Onori, F., et al. 2020, *SSRv*, 216, 124
- Wevers, T., Pasham, D., van Velzen, S., et al. 2019, *MNRAS*, 488, 4816